Received: 2 October 2017 | Accepted: 1 March 2019

DOI: 10.1002/hyp.13448

RESEARCH ARTICLE

WILEY

Improvement of surface run-off in the hydrological model ParFlow by a scale-consistent river parameterization

Bernd Schalge[1] | Vincent Haefliger[1] | Stefan Kollet[2,3] | Clemens Simmer[1,3]

[1] Institut für Geowissenschaften und Meteorologie, Bonn Universität, Bonn, Germany

[2] Forschungszentrum Jülich IBG-3, Jülich, Germany, Jülich, Germany

[3] Centre for High-Performance Scientific Computing in Terrestrial Systems, Geoverbund, ABC/J, Jülich, Germany

Correspondence
Bernd Schalge, Institut für Geowissenschaften und Meteorologie, Bonn Universität, 176 Meckenheimer Allee, 53115 Bonn, Germany
Email: bschalge@uni-bonn.de

Funding information
Deutsche Forschungsgemeinschaft (DFG)

Abstract

We propose an improvement of the overland-flow parameterization in a distributed hydrological model, which uses a constant horizontal grid resolution and employs the kinematic wave approximation for both hillslope and river channel flow. The standard parameterization lacks any channel flow characteristics for rivers, which results in reduced river flow velocities for streams narrower than the horizontal grid resolution. Moreover, the surface areas, through which these wider model rivers may exchange water with the subsurface, are larger than the real river channels potentially leading to unrealistic vertical flows. We propose an approximation of the subscale channel flow by scaling Manning's roughness in the kinematic wave formulation via a relationship between river width and grid cell size, following a simplified version of the Barré de Saint-Venant equations (Manning–Strickler equations). The too large exchange areas between model rivers and the subsurface are compensated by a grid resolution-dependent scaling of the infiltration/exfiltration rate across river beds. We test both scaling approaches in the integrated hydrological model ParFlow. An empirical relation is used for estimating the true river width from the mean annual discharge. Our simulations show that the scaling of the roughness coefficient and the hydraulic conductivity effectively corrects overland flow velocities calculated on the coarse grid leading to a better representation of flood waves in the river channels.

KEYWORDS

channel flow, flood forecasting, hydrological modelling, infiltration processes, scaling overland flow

1 | INTRODUCTION

Surface water storage and fluxes in rivers, lakes, reservoirs, and wetlands are currently poorly observed at the regional scale, even though they represent major components of the water cycle and strongly impact human societies (Biancamaria & Pavelsky, 2016) in terms of water resources and extreme events such as floods. In situ observation networks are heterogeneously distributed in space, and many river basins and most lakes—especially in the developing world and sparsely populated regions—remain unmonitored (Biancamaria et al., 2010).

The mass balance equation regulating the continental water cycle relates on arbitrary spatial scales, the temporal total water storage variation to the water fluxes between the land surface, the atmosphere,

and the subsurface described by precipitation, evapotranspiration, infiltration into the subsurface, exfiltration to the surface, and overland flow. Physically-based distributed hydrological models simulate the evolution in time and space of the state variables and fluxes, and can be used to calculate and predict discharge and/or water levels at each grid-column and time-step and to compensate for the lack of sufficient observations. Observations are, however, required for model calibration, initialization, and validation.

In this paper, we focus on overland flow as part of the hydrometeorological system. Several methods exist for simulating overland flow such as the Saint-Venant equations or approximations thereof like kinematic or diffusive waves. Even simpler routing methods exist based only on source and sink terms (Clark et al., 2017, 2015; de Rooij, 2017). Some models calculate overland flow at the grid scale, whereas others use routing schemes for separate channels not related to the grid resolution. We target the prior model types for which grid scales are usually much larger than the size of the real rivers. Realistic overland flow simulations despite low spatial resolutions would limit the usually high computational demand of such models (Clark et al., 2015). Much higher resolutions—and thus substantially increased IT resources—are required when the scale dependence of lateral fluxes are explicitly taken into account (Wood et al., 2011).

The distributed model ISBA/MODCOU (Masson et al., 2013, Ledoux, Girard, Marsily, & Deschenes, 1989, David, Habets, Maidment, & Yang, 2011, David et al., 2011, Häfliger et al., 2015) is one example of the model type discussed; the model is used to simulate discharge and river water levels over France. Other examples are the global-scale Catchment-based Macroscale Floodplain (CaMa-Flood; Yamazaki, de Almeida, & Bates, 2013) and the ISBA–TRIP (Decharme et al., 2012) models, which are run at relatively low resolution but use subscale digital elevation model (DEM) information to characterize floodplain areas within individual grid cells. The limited resolution of such regional or large scale models requires the parameterization of subgrid scale processes especially for overland flow and river routing. Neal, Schumann, and Bates (2012) studied the effect of subgrid scale channel routing on flood dynamics by using a hydraulic model for the Niger River in Mali, which allows for river channels of any width; they showed that more detailed (smaller) channels considerably improved model performance.

An alternative to explicit sub-grid channel routing is the scaling of relevant parameters in grid-scale river routing models. Schalge et al. (2017) show that without any scaling, the grid-scale routing scheme at a resolution of 400 m delays the discharge peak at the mouth of the Neckar catchment (south-western Germany) by 3 days, whereas peaks are underestimated compared with observations. Sub-scale parameterizations have been developed based on the subgrid scale topographic index, for example, by Niedda (2004), which has been refined, for example, by Fang, Bogena, Kollet, and Vereecken (2016), and shown to improve river discharge. Other methods employ probabilistic approaches (Piccolroaz et al., 2016) to account for uncertainty related to overland flow.

In this study, we propose an improvement of the overland-flow parameterization for distributed hydrological models with constant horizontal grid resolution, which employ the kinematic wave approximation for both hillslope and river channel flow. Without subscale parameterization, such models simulate reduced river flow velocities for streams narrower than the horizontal grid resolution. Moreover, surface areas, through which these wider model rivers may exchange water with the subsurface, are larger than the real river channels potentially leading to unrealistic vertical flows. We propose an approximation of the subscale channel flow by scaling Manning's roughness in the kinematic wave formulation via a relationship between river width and grid cell size following a simplified version of the Barré de Saint-Venant equations (Manning–Strickler equations, see Section 2.2 for details). The too-large exchange areas between model rivers and the subsurface are compensated by a grid resolution-dependent scaling of the infiltration/exfiltration rate across river beds for the top layer. Both the roughness coefficient and the hydraulic conductivity can be objectively scaled by assuming a rectangular river channel cross section with variable width embedded in the fixed-size river grid cells. The approach is simple to implement and requires no additional computational demand.

We implemented the approach in the distributed hydrological model ParFlow (Kollet & Maxwell, 2006), which simulates surface run-off and subsurface flow processes, and was also used in Schalge et al. (2017). ParFlow uses the same equally-spaced horizontal grid for 3D subsurface flow and 2D overland flow. For computational reasons, the horizontal resolution is on the order of several hundred metres if run over medium (~50,000 km^2) or large-scale (>150,000 km^2) catchment sizes. To our knowledge, such an approach has not been tested before to improve river behaviour, though a similar approach has been recently used to infer a scaling law for hydraulic conductivity for entire catchments by Foster and Maxwell (2019).

The ParFlow model is introduced briefly in Section 2, with a focus on shallow overland flow and variably saturated groundwater flow and on its integration in the fully coupled land surface-atmosphere modelling framework TerrSysMP. Our scaling approaches for Manning's coefficient and hydraulic conductivity are described in Section 3. After presenting the experimental design in Section 4, we demonstrate in Section 5 the usefulness of the approach in synthetic numerical experiments and in an application to the real-world Neckar catchment in southern Germany. Section 6 summarizes the results and concludes with implications and suggestions for future studies.

2 | THE PARFLOW MODEL

ParFlow is a 3D variably saturated groundwater flow model with a free-surface overland flow boundary condition (Jones & Woodward, 2001; Kollet & Maxwell, 2006). In a continuum approach, ParFlow is used to simulate the coupled surface–subsurface hydrodynamics, including the redistribution of soil moisture and the flow of groundwater and surface water in an integrated fashion.

2.1 | Variably saturated groundwater flow

The mass balance of variably saturated flow following Richards (1931) relates the temporal variation of the degree of saturation S_w [−] in soil to the water (Darcy) flux divergence q [L T^{-1}]. Assuming no sinks or sources in the domain this yields,

$$\frac{dS_w}{dt} = -\vec{\nabla}\cdot\vec{q}, \tag{1a}$$

$$\vec{q} = -K_{\text{sat}}\cdot k_r(\psi)\cdot\vec{\nabla}\left(\psi_p + z\right), \tag{1b}$$

with K_{sat}, [L T^{-1}] is the three-dimensional, spatially variable saturated hydraulic conductivity, ψ_p [L] is the subsurface pressure head, k_r [−] is the relative permeability depending on pressure head ψ_p, and z [L] is the gravitational potential with the positive z-axis pointing upward. The hydraulic conductivity K_{sat} depends on soil texture, which is parameterized in ParFlow by the van Genuchten relationship (Van Genuchten, 1980):

$$S_w\left(\psi_p\right) = \frac{S_{\text{sat}} - S_{\text{res}}}{\left(1 + \left(\alpha\cdot\psi_p\right)^{\beta}\right)^{(1-1/\beta)}} + S_{\text{res}}, \tag{2a}$$

$$k_r\left(\psi_p\right) = \frac{\left(1 - \frac{\left(\alpha\cdot\psi_p\right)^{\beta-1}}{\left(1+\left(\alpha\cdot\psi_p\right)^{\beta}\right)^{(1-1/\beta)}}\right)^2}{\left(1 + \left(\alpha\cdot\psi_p\right)^{\beta}\right)^{\frac{(1-1/\beta)}{2}}}, \tag{2b}$$

with α [L^{-1}] and β [−] as soil parameters, S_{sat} [−] is the relative saturated water content, and S_{res} [−] is the residual saturation. More details on the subsurface physics and numerical implementation of ParFlow can be found in Jones and Woodward (2001).

2.2 | Shallow overland flow

The solution of the Barré de Saint-Venant equations describes the routing of water over a rough surface. In general, the resulting flood wave has advective and diffusive properties. The kinematic wave approximation, which is used in ParFlow, neglects the diffusive part. Under this assumption, Manning's equation can be used to establish a flow depth–discharge relationship for a rectangular river channel of the form

$$v = \frac{1}{n}\cdot\sqrt{S_f}\cdot\psi^{2/3}, \tag{3a}$$

$$\psi = \left(\frac{Q\cdot n}{W\cdot\sqrt{S_f}}\right)^{3/5}, \tag{3b}$$

where Q is the river discharge [L^3 T^{-1}], v is the average flow velocity [L T^{-1}], ψ is the surface pressure head (or ponding depth) [L], n is the Manning's coefficient [T $L^{-1/3}$], S_f is the bed slope [L L^{-1}], and W is the river width [L].

In ParFlow, overland flow is incorporated via an overland flow boundary condition assuming pressure and flux continuity at the surface–subsurface interface (Kollet & Maxwell, 2006). Thus, the system of equations of variably saturated groundwater and overland flow is coupled via the boundary condition at the ground surface leading to

$$-K_s(x, y, z)\cdot k_r(\psi)\cdot\vec{\nabla}\left(\psi_p + z\right) = \frac{\partial||\psi, 0||}{\partial t} - \vec{\nabla}\cdot\vec{v}\,||\psi, 0||, \tag{4}$$

with ||A,B|| the greater of A and B. Pressure head continuity ($\psi_s = \psi_p = \psi$) states that the pressures of the surface and subsurface domains vary continuously across the land surface.

2.3 | Integration of ParFlow in the Terrestrial Systems Modelling Platform (TerrSysMP)

ParFlow is the hydrological component of the Terrestrial Systems Modelling Platform (TerrSysMP; Shrestha, Sulis, Masbou, & Simmer, 2014), which has been used for hydrological and regional climate applications on small (Shrestha, Sulis, Simmer, & Kollet, 2015), medium (Sulis et al., 2017; Sulis, Keune, Shrestha, Simmer, & Kollet, 2018), and large scale catchments (Keune et al., 2016), including a parallel data assimilation approach (Kurtz et al., 2016). TerrSysMP couples ParFlow, the Community Land Model (CLM; Oleson et al., 2008), and the numerical weather prediction model Consortium for Small Scale Modelling (COSMO; Baldauf et al., 2011) via the Ocean Atmosphere Sea Ice Coupling (OASIS3) framework (e.g., Valcke, 2006) and OASIS3-MCT (Gasper et al., 2014). CLM is a single-column bio geophysical land-surface model considering coupled snow-processes, soil-processes, and vegetation-processes simulating the water, energy, and momentum balances at the land surface and released by the National Center for Atmospheric Research (NCAR). COSMO is a non-hydrostatic atmosphere model, which is operationally applied at the German (DWD) and other national weather services for weather prediction. Thus, TerrSysMP allows simulating the terrestrial water, energy, and biogeochemical cycles from the deeper subsurface including groundwater (ParFlow) across the land-surface (CLM) into the atmosphere (COSMO). Water and energy cycles are coupled via, for example, evaporation and plant transpiration; these processes are modelled by CLM with a coupling to ParFlow through soil-water availability and root-water uptake.

3 | RIVER PARAMETERIZATION

ParFlow does not differentiate between hillslope run-off and river flow, for example, by accounting for specific channel geometries, and the same horizontal grid resolution applies both for the subsurface and surface water domains. Because especially the latter depends on unresolved subgrid scale surface topography, negative effects on water flow may result. This could be compensated either by incorporating subgrid scale river channel geometries, including the relevant exchange fluxes with the subsurface, for example, via conductance concepts or by scaling grid-scale parameters according to the used

resolution. In order to utilize the overland flow boundary condition in ParFlow, we explore the latter option and derive grid resolution-dependent scalings of the Manning's coefficient n and the saturated hydraulic conductivity K_{sat}.

3.1 | Scaling the Manning's coefficient

The proposed scaling of the Manning's coefficient n adjusts the flow velocity v in a grid cell with a river channel to the flow velocity in a "true" river channel of smaller width W. n can be objectively scaled by assuming a rectangular river channel cross section with a certain width contained in the larger river grid cell (Figure 1). Let the true situation (given, e.g., by a high resolution simulation) be a river channel of width W_1 with a Manning's coefficient n_{org} and a flow velocity v_1. In a coarser-scale model, the river has a (wider) width W_2 equal to the width of the grid cell. The original Manning's coefficient n_{org} will then result in a lower flow velocity v_2 (compared with v_1) because of the smaller water depth in the wider channel. Whereas keeping the model river width at W_2 (the size of a coarse grid cell), we scale (reduce) the original Manning's coefficient n_{org} to n_{scale}, such that the resulting flow velocity v_3 is equal to the true velocity v_1. In order to obtain n_{scale}, we impose for all three cases the same discharge Q in the upstream part of the respective virtual channel; thus from Equation (3) follows

$$\psi_1 = \left(\frac{Q \cdot n_{org}}{W_1 \cdot \sqrt{S_f}}\right)^{3/5}, \tag{5a}$$

$$v_1 = \frac{1}{n_{org}} \cdot \sqrt{S_f} \cdot \psi_1^{2/3}, \tag{5b}$$

where ψ_1 is the true ponding depth of the river. With the same Manning's coefficient n_{org} and discharge Q. For a larger (model) river width W_2 follows in the same manner a smaller ponding depth ψ_2 of the model river. Because $W_2 > W_1$ and $\psi_2 < \psi_1$, it follows $v_2 < v_1$. We require from the scaled Manning's coefficient n_{scale}, that the original (true) flow velocity is conserved ($v_3 = v_1$). Using n_{scale} in (5a) and (5b) yields

$$\frac{1}{n_{scale}} \cdot \sqrt{S_f} \cdot \left(\frac{Q \cdot n_{scale}}{W_2 \cdot \sqrt{S_f}}\right)^{2/5} = \frac{1}{n_{org}} \cdot \sqrt{S_f} \cdot \left(\frac{Q \cdot n_{org}}{W_1 \cdot \sqrt{S_f}}\right)^{2/5}, \tag{6}$$

which can be solved for the scaled Manning's coefficient n_{scale}

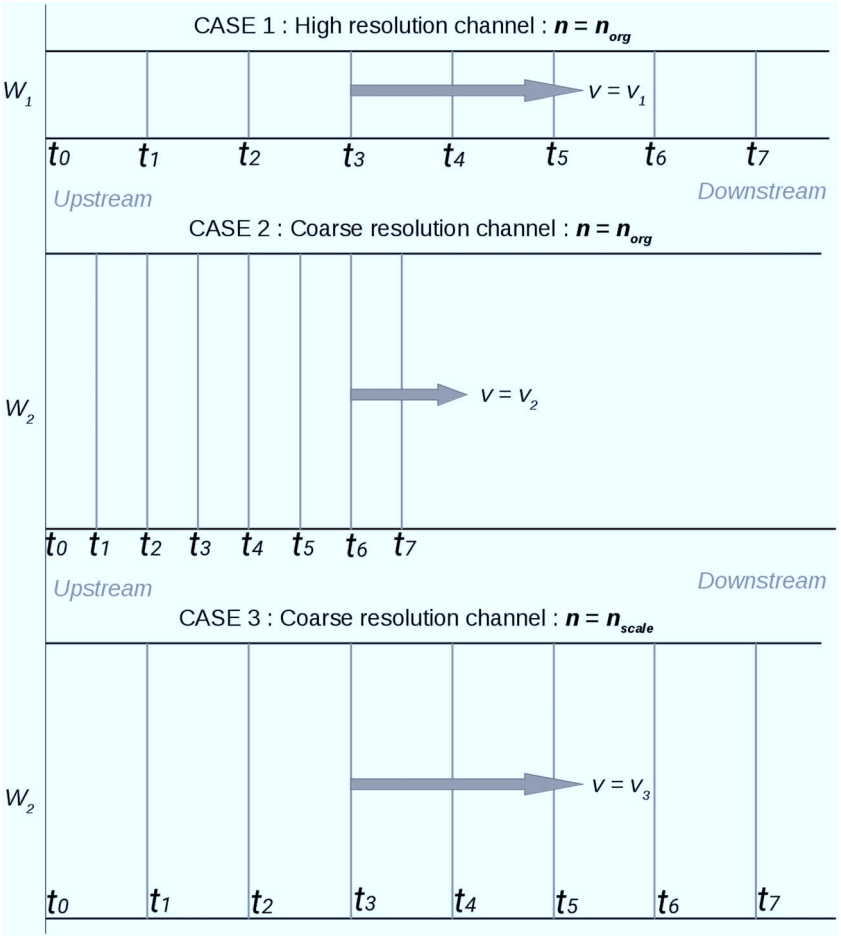

FIGURE 1 Illustration of the scaling concept for the Manning's coefficient (see text). W_1 is the true channel width and W_2 the (wider) width of the grid cell and thus the model river width. The flow velocities v_i are indicated by the length of the grey arrows and the vertical lines represent the position of peak discharge at each time step tn

$$n_{\text{scale}} = n_{\text{org}} \cdot \left(\frac{W_1}{W_2}\right)^{2/3} = \lambda \cdot n_{\text{org}}. \quad (7)$$

In Equation (7), $\lambda = \left(\frac{W_1}{W_2}\right)^{2/3}$ is the scaling coefficient for Manning's coefficient, which results in the original (true) river flow velocity for a model channel width W_2 independent of channel slope S_f and discharge Q.

3.2 | Scaling the hydraulic conductivity

Because the model river width is typically larger than the true river width, a larger surface area will exchange water with the subsurface compared with the real river. This can be corrected by using a scaled (reduced) hydraulic conductivity $K_{\text{sat scale}}$ (scaled K_{sat}, case 4 in Figure 2). Conserving the original (true) infiltration/exfiltration fluxes $Q_{\text{in/ex}}$ ($Q_{\text{in/ex case 4}} = Q_{\text{in/ex case 1}}$) requires the following:

$$\int_{A_4} K_{\text{satscale}} dA_4 = \int_{A_1} K_{\text{satorg}} dA_1, \quad (8)$$

with A [L^2] as the horizontal area of the river in the grid cell ($A_1 = W_2 \times W_1$ for case 1; $A_4 = W_2 \times W_2$ for scaled K_{sat}, assuming square grid cells) leading to

$$\int_0^{W_2}\int_0^{W_2} K_{\text{satscale}}(x, y)dxdy = \int_0^{W_2}\int_0^{W_1} K_{\text{satorg}}(x, y)dxdy. \quad (9)$$

Assuming a homogeneously distributed hydraulic conductivity K_{sat} over the entire grid cell, we get

$$K_{\text{satscale}} \cdot W_2 \cdot W_2 = K_{\text{satorg}} \cdot W_2 \cdot W_1, \quad (10)$$

and finally

$$K_{\text{satscale}} = K_{\text{satorg}} \cdot \frac{W_1}{W_2}, \quad (11)$$

with $\varkappa = \frac{W_1}{W_2}$ as the scaling coefficient for the hydraulic conductivity.

4 | EXPERIMENTAL DESIGN

In order to verify the proposed scaling of n and K_{sat}, an idealized and a real-world test case were implemented in ParFlow. The idealized test case considers a simple domain where the truth (high resolution) is known. Thus, we can directly validate both the approach and its implementation in ParFlow. The real-world test case is set up for the Rhine-Neckar area in order to evaluate the approach by comparison with real observations. Here, we are faced with realistic heterogeneity, which leads to additional nonlinear feedbacks of the scaled parameterizations with the model. Although a direct comparison with observations is difficult due to additional uncertainties in the real land surface processes and meteorological forcings, we can use the results discussed in Schalge et al. (2017) to evaluate whether our scaling approach generates the expected changes in the catchment response.

4.1 | Idealized test case

The idealized test case (Figure 3) is a rectangular model area, which encompasses a channel of length L_y = 50 km connected to a hill slope of width L_x = 25 km, with a slope S_o^x = 0.01 m m^{-1} in x-direction and S_o^y = 0.0001 m m^{-1} in y-direction. The channel has a zero slope in x-direction, $S_f^x = 0$, and slopes downward with S_f^y = 0.0001 mm^{-1} in y-direction. The horizontal model resolution is $dx = dy$ = 40 m for the high resolution and $Dx = Dy$ = 100/200/400 m for the three other cases. The tilted model domain has a depth L_z of 100 m divided into 50 vertical layers, with a resolution starting at 1 cm at the top and increasing to 4 m at the bottom. All hydraulic parameters are assumed

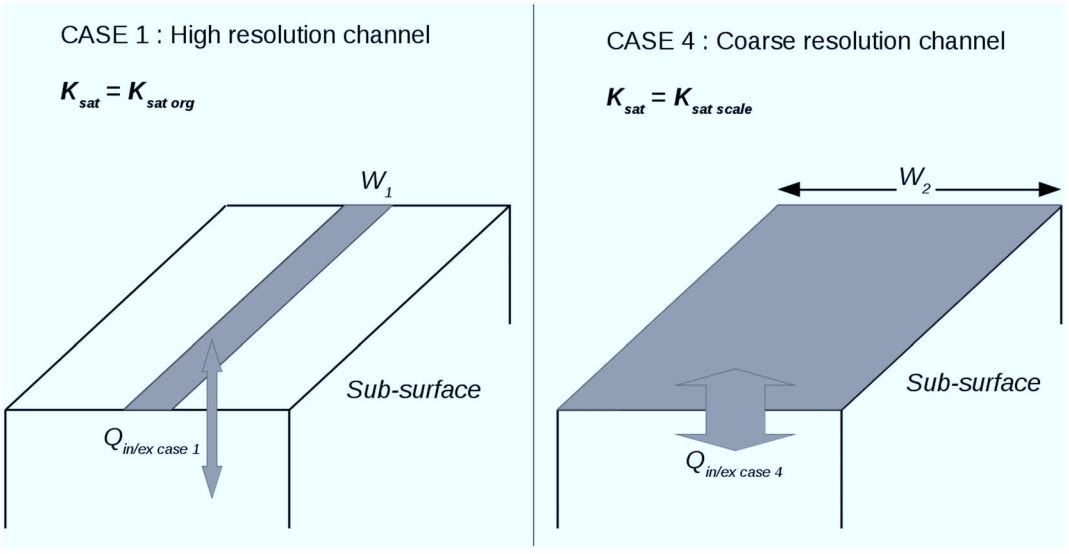

FIGURE 2 Schematic for the scaling of the hydraulic conductivity (see text) with $K_{\text{sat org}}$ the original saturated conductivity and $K_{\text{sat scale}}$ its scaled counterpart. Qin/ex [L3 T^{-1}] represents the infiltration or exfiltration flux between the river and the subsurface

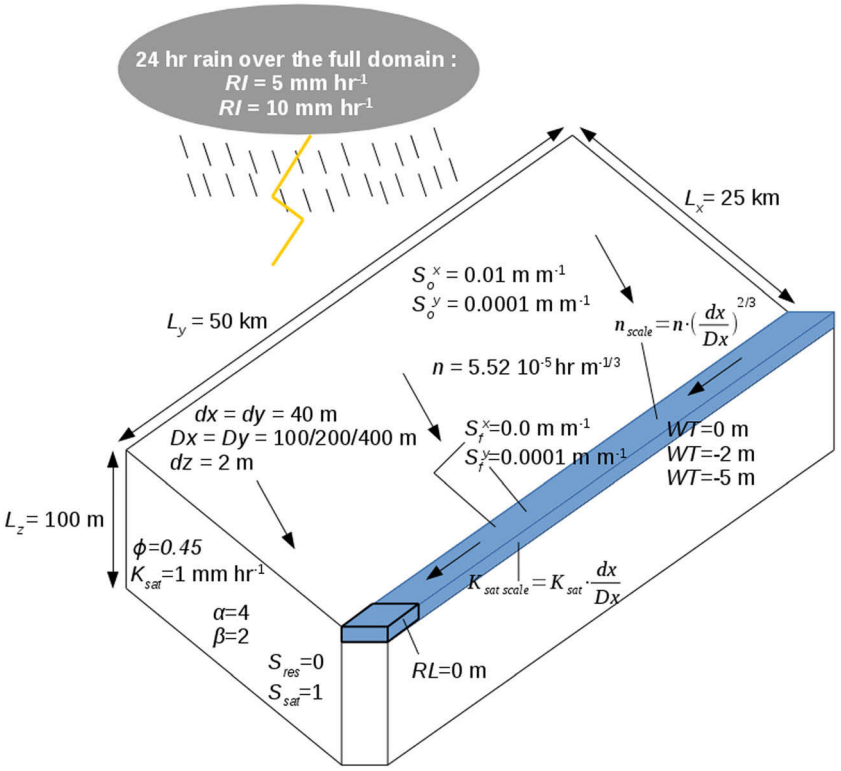

FIGURE 3 Idealized test case with spatial dimensions L_x, L_y, L_z vertical resolution d_z and horizontal resolutions d_x and d_y, or D_x and D_y, depending on the case. Different hydrostatic initial conditions of the pressure head ψ are represented by different water table elevations (WT) at the reference level at the outlet of the river (RL, marked gridcell). Additional symbols are defined in the main text. The arrows indicate the main overland flow directions at the hillslope and in the channel

constant over the whole model domain, with values for porosity ϕ [−] = 0.45, van Genuchten parameters α = 4 $m^{-1,}$ β = 2, S_{res} = 0, and S_{sat} = 1, hydraulic conductivity K_{sat} = 0.001 m hr^{-1}, and Manning's coefficient n = 5.52 × 10^{-5} hr $m^{-1/3}$. The hydrograph behaviour is analysed in the bottom left corner of the box, corresponding to the river outlet. The scaling parameters λ and $\varkappa$ are calculated from the ratio dx/Dx via Equation (7) and (11).

In total, 78 experiments were performed with the idealized test case. These encompass two rain intensities (0.005 and 0.010 m hr^{-1}, constant in space and time and applied during the first 24 simulation hours) and three hydrostatic initial conditions (water table elevations (*WT*) of −5, −2, and 0 m, with respect to the reference elevation of *RL* = 0 m at the channel outlet, marked grid cell in Figure 3). These six cases were simulated without scaling, with scaled Manning's coefficient, with scaled hydraulic conductivity, and with both scalings implemented, for the three spatial resolutions resulting in 78 cases total. Table 1 shows all experiment setups and can be used as further reference with regard to the names of the different cases.

4.2 | Semi-idealized real-world case: The Neckar catchment area

4.2.1 | Catchment description

The real-world Neckar catchment model encompasses about 14,000 km^2, was originally developed by Schalge et al. (2017), and is located in the southwest of the German state Baden-Württemberg, east of the Black Forest, and north of the Swabian Alb. The Neckar river passes the cities of Tübingen, Stuttgart, and Eberbach, and discharges into the Rhine at Mannheim. Its main tributaries are the Fils, Rems, Enz, Kocher, and Jagst rivers (Figure 4, from Bürger et al., 2006). The topography ranges from 90 to 1,050 m and the mean annual precipitation between 600 and 2000 mm with the highest values over the Black Forest. Daily average temperatures vary with altitude between −5°C and 0°C in January and 13°C and 18°C in July. At lower elevations, land use and cover are dominated by agriculture, whereas the Black Forest features mainly needle-leaf trees. Broad-leaf trees can be found over smaller areas throughout the catchment. Average groundwater levels are less than two metres below the land surface for large areas suggesting strong coupling between groundwater and evapotranspiration. The soil texture in the superficial soil is mainly clay in the plain area and sand over the black forest mountains. Soil texture is taken from the soil map (BUEK1000) of the Rhine-Neckar as provided by the Federal Institute for Geosciences and Natural Resources—BGR (http://www.bgr.bund.de/DE/Themen/Boden/Informationsgrundlagen/Bodenkundliche_Karten_Datenbanken/BUEK1000/buek1000_node.html).

4.2.2 | Model configuration

1. Time and space resolution

ParFlow runs with a horizontal resolution of 400 m, which results in 535 grid cells in the *x*-direction and 605 grid cells in the *y*-direction. Vertically, the model has, similar to the idealized model setup, 50 layers with a resolution starting at 1 cm at the top and increasing to 4 m at the bottom. The time step is 900 s, and pressure head and soil water content are output every 3 hr.

TABLE 1 Setups of all experiments performed

Experiment	dx/dy	WT [m]	Manning's	Ksat	rain rate
Ex1	40	0	−	−	0.005
Ex2	40	−2	−	−	0.005
Ex3	40	−5	−	−	0.005
Ex4	40	0	−	−	0.01
Ex5	40	−2	−	−	0.01
Ex6	40	−5	−	−	0.01
Ex7	100	0	−	−	0.005
Ex8	100	−2	−	−	0.005
Ex9	100	−5	−	−	0.005
Ex10	100	0	−	−	0.01
Ex11	100	−2	−	−	0.01
Ex12	100	−5	−	−	0.01
Ex13	100	0	+	−	0.005
Ex14	100	−2	+	−	0.005
Ex15	100	−5	+	−	0.005
Ex16	100	0	+	−	0.01
Ex17	100	−2	+	−	0.01
Ex18	100	−5	+	−	0.01
Ex19	100	0	−	+	0.005
Ex20	100	−2	−	+	0.005
Ex21	100	−5	−	+	0.005
Ex22	100	0	−	+	0.01
Ex23	100	−2	−	+	0.01
Ex24	100	−5	−	+	0.01
Ex25	100	0	+	+	0.005
Ex26	100	−2	+	+	0.005
Ex27	100	−5	+	+	0.005
Ex28	100	0	+	+	0.01
Ex29	100	−2	+	+	0.01
Ex30	100	−5	+	+	0.01
Ex31	200	0	−	−	0.005
Ex32	200	−2	−	−	0.005
Ex33	200	−5	−	−	0.005
Ex34	200	0	−	−	0.01
Ex35	200	−2	−	−	0.01
Ex36	200	−5	−	−	0.01
Ex37	200	0	+	−	0.005
Ex38	200	−2	+	−	0.005
Ex39	200	−5	+	−	0.005
Ex40	200	0	+	−	0.01
Ex41	200	−2	+	−	0.01
Ex42	200	−5	+	−	0.01
Ex43	200	0	−	+	0.005
Ex44	200	−2	−	+	0.005
Ex45	200	−5	−	+	0.005
Ex46	200	0	−	+	0.01
Ex47	200	−2	−	+	0.01
Ex48	200	−5	−	+	0.01
Ex49	200	0	+	+	0.005
Ex50	200	−2	+	+	0.005
Ex51	200	−5	+	+	0.005
Ex52	200	0	+	+	0.01
Ex53	200	−2	+	+	0.01
Ex54	200	−5	+	+	0.01
Ex55	400	0	−	−	0.005
Ex56	400	−2	−	−	0.005
Ex57	400	−5	−	−	0.005
Ex58	400	0	−	−	0.01
Ex59	400	−2	−	−	0.01
Ex60	400	−5	−	−	0.01
Ex61	400	0	+	−	0.005
Ex62	400	−2	+	−	0.005
Ex63	400	−5	+	−	0.005
Ex64	400	0	+	−	0.01
Ex65	400	−2	+	−	0.01
Ex66	400	−5	+	−	0.01
Ex67	400	0	−	+	0.005
Ex68	400	−2	−	+	0.005
Ex69	400	−5	−	+	0.005
Ex70	400	0	−	+	0.01
Ex71	400	−2	−	+	0.01
Ex72	400	−5	−	+	0.01
Ex73	400	0	+	+	0.005
Ex74	400	−2	+	+	0.005
Ex75	400	−5	+	+	0.005
Ex76	400	0	+	+	0.01
Ex77	400	−2	+	+	0.01
Ex78	400	−5	+	+	0.01

2. Hydrological parameters

Although hydraulic conductivity varies spatially in ParFlow, the specific storage value is set constant in the domain with a value of S_s = 0.001. The slopes are obtained from the European Environmental Agency-Digital Elevation Model (EEA-DEM). The van Genuchten parameters α and β are calculated from the soil type based on the BUEK1000 map; this results in low values for clay soils with low hydraulic conductivity mainly in the plain area, whereas high values for sandy soils with high hydraulic conductivity dominate in the black forest mountains. The Manning's coefficient is assumed constant over

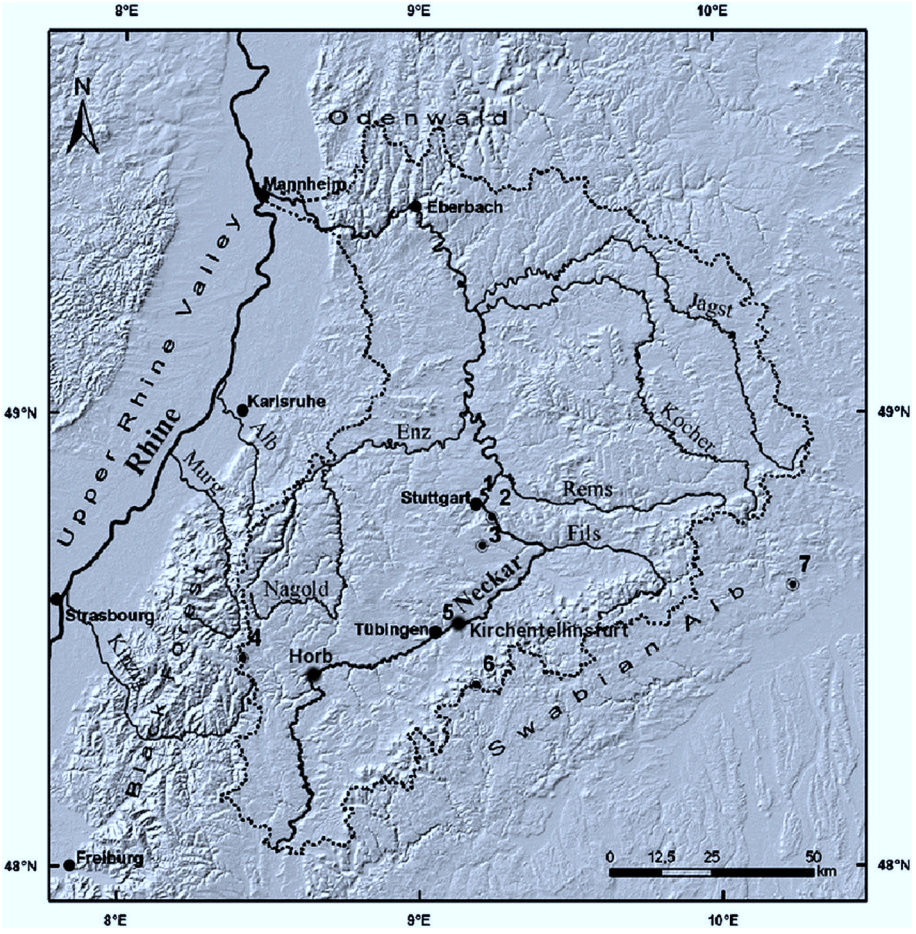

FIGURE 4 Rhine-Neckar model area (Bürger et al., 2006), including the main tributaries and urban areas. The grey dotted line delineates the Neckar catchment

the full domain with $n = 5.52 \times 10^{-5}$ hr $m^{-1/3}$. The hydraulic conductivity K_{sat} ranges from 0.001 to 0.1 m hr^{-1} in the surface layer.

3. Initialization and experimental set-up

The initial condition for pressure head ψ is obtained from a 5-year TerrSysMP spinup simulation using repeated atmospheric forcing of the calendar year 2007. The spinup starts with a hydrostatic (no vertical flow) condition with a water table at 2 m below the land surface. During spinup, the pressure head ψ adjusts to the atmospheric forcing resulting in, for example, positive values along river corridors (water ponding) and negative values in hill slope areas when no overland flow is happening.

In order to evaluate the proposed scaling approach, a numerical experiment was performed where ParFlow was applied in stand-alone mode. A virtual meteorology was imposed on the system, taking into account only the precipitation for the calculation of the run-off/infiltration partitioning. The other meteorological variables like temperature, wind, or solar radiation are not considered, and evapotranspiration is set to zero in this experiment. During the two first weeks of the simulation, no rain was imposed to the system, followed by 12 hr (between hours 336 and 348, day 14 to 14.5) of uniform rain of 1 mm hr^{-1} intensity over the full domain. For the following 2 weeks (between hours 348 and 684, day 14.5 to 28.5), the discharge following the rain event was analysed at the Neckar outlet to the Rhine at Mannheim.

4.2.3 | Scaling for the Neckar catchment area

In order to scale the hydraulic parameters via Equations (7) and (11) for each river grid cell, the true river widths (W_1) are needed, which we set to an effective river width W_1, estimated from known upstream discharge values via an empirical relationship by Leopold and Maddock (1953) as a function of the mean annual discharge Q,

$$W_1 = k \cdot Q^m, \tag{14}$$

with k = 7.12 and m = 0.53. The parameters k and m were fitted, tested, and validated by Häfliger et al. (2015) for the Garonne catchment (55,846 km^2), whose catchment area is close to the simulated domain (57,850 km^2), covering all the Rhine-Neckar area. Figure 5 shows the resulting effective river width (spatial and cumulative distribution) for the Rhine-Neckar area, which varies between 10 and 150 m, with a mean width of about 34.5 m and a standard deviation

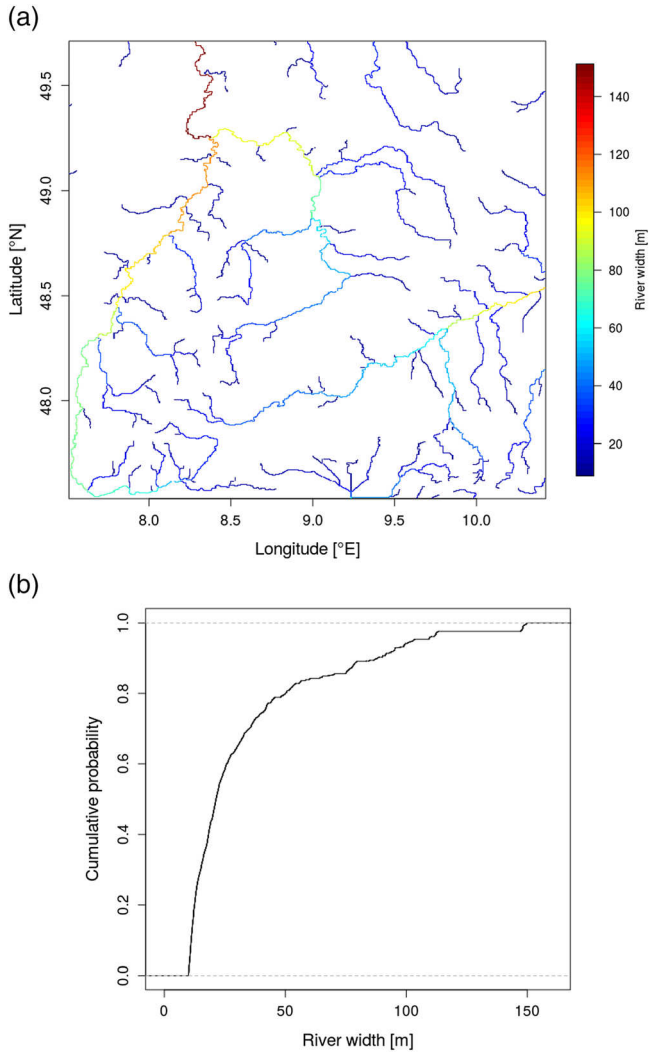

FIGURE 5 (a) Effective river width W_1 [m] > 10 m for the Rhine-Neckar area, (b) cumulative distribution function of effective river width for W_1 > 10 m

of 31.5 m. River widths below 10 m (contained in 96.6% of all surface grid cells) are not taken into account, because rivers narrower than 10 m will show up in a 400 m resolution topography as gridcells with overland flow only during and shortly after rain events, but not, for example, during dry spells. Discharge from such small rivers varies significantly in time, whereas the average flow is very small preventing a reliable stream width estimate. In addition, several small streams would be present on one grid cell, which cannot be modelled with this approach.

The resulting scaling parameter λ for Manning's coefficient following Equation (9) ranges from 0.1 in mountainous areas to 0.5 in the lowlands. For example, the Manning's coefficient for a 10 and a 150-m wide river would be scaled by 0.1 and 0.5, respectively, in order to result in flow velocities comparable with those of the true rivers. The scaled Manning's coefficient n_{scale} (Figure 6) ranges from 0.5×10^{-5} hr $m^{-1/3}$ in mountain rivers to 2.7×10^{-5} hr $m^{-1/3}$ in the lowland. The scaling parameter ν for the hydraulic conductivity $K_{sat\ org}$ ranges from 0.025 in the mountains to 0.33 in the lowlands. For

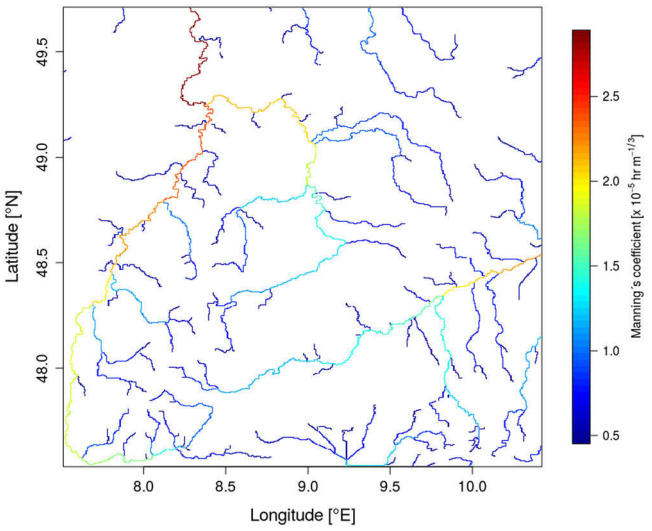

FIGURE 6 $K_{sat\ scale}$ in units of log10 [m hr^{-1}] for the Neckar area

example, the hydraulic conductivity $K_{sat\ org}$ for a 10-m and a 150-m wide river would be scaled by 0.025 and 0.3, respectively, in order to result in in/exfiltration rate comparable with those of the true rivers. The resulting scaled coefficients $K_{sat\ scale}$ range from 0.5 mm hr^{-1} in mountain rivers to 6 mm hr^{-1} in low lands.

5 | RESULTS

5.1 | Idealized testcase

In all figures showing results of the idealized test case setup for different spatial resolutions, the Nash-Sutcliffe Criterion (NSC) (Nash & Sutcliffe, 1970) was computed by taking the results of the high resolution (40 m) setup as observations. Figure 7 compares the hydrograph at the channel outlet simulated at the 40 m resolution for the three initial water table conditions for the low rain case. The initial condition has only a small impact on the discharge characteristics, whereas the effect of a higher infiltration can be observed for the low water table case. For the high rain case, the results for all setups become indistinguishable (not shown).

Figure 8 compares the results from the simulations for the different resolutions without scaling for the high water table initial condition and the low rain rate. Already when lowering the resolution from 40 to 100 m almost halves the discharge amplitude and significantly slows down recession afterwards (NSC = 0.46). As expected, differences drastically increase for the 200 m (NSC = −1.29) and the 400 m resolution (NSC = −4.41). In addition, for the high rain rate case (Figure 9), the peak discharge time is increasingly delayed while coarsening the resolution. The much more pronounced peaks of the hydrographs for the higher rain rate, however, results in NSCs of 0.83 for the 100 m case, 0.33 for the 200 m case, and −0.81 for the 400 m case.

The effect of the different scaling applied at 400 m resolution is shown in Figure 10. For a high water table and a low rain rate, the scaling of the hydraulic conductivity alone has little impact; only

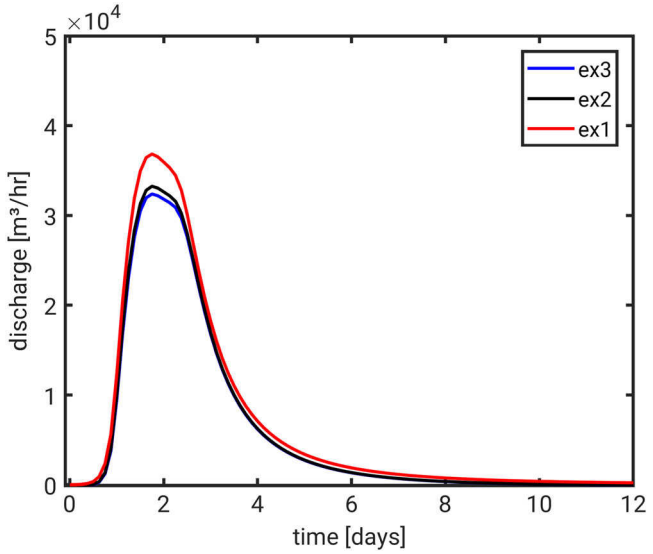

FIGURE 7 Hydrographs for the 40 m resolution case with low rain rate (0.005 mm/hr) for the three different initial conditions with WT = 0 m (ex1), WT = −2 m (ex2), and WT = −5 m (ex3)

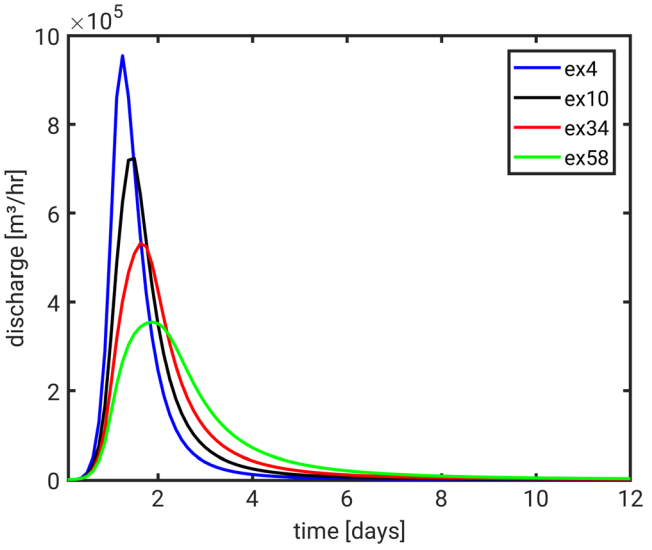

FIGURE 9 Hydrographs for the case with high rain rate (0.01 mm/hr) and WT = 0 m initial conditions without any scaling for the resolutions 40 m (ex4), 100 m (ex10), 200 m (ex34), and 400 m (ex58)

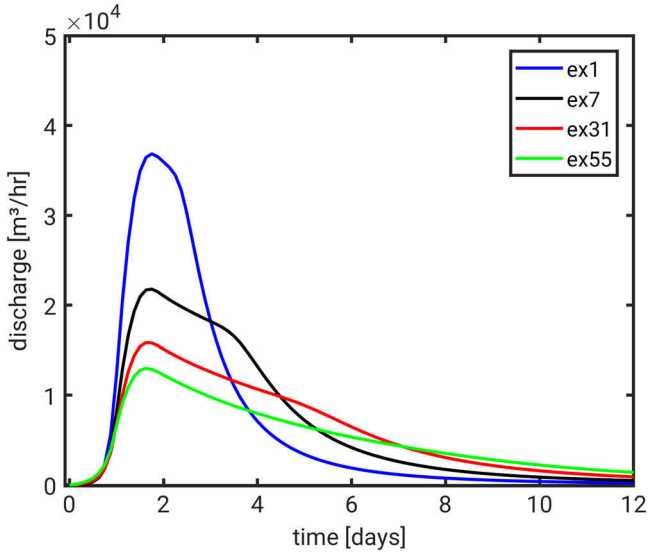

FIGURE 8 Hydrographs for the case with low rain rate (0.005 mm/hr) and WT = 0 m initial conditions without any scaling for the resolutions 40 m (ex1), 100 m (ex7), 200 m (ex31),0 and 400 m (ex55)

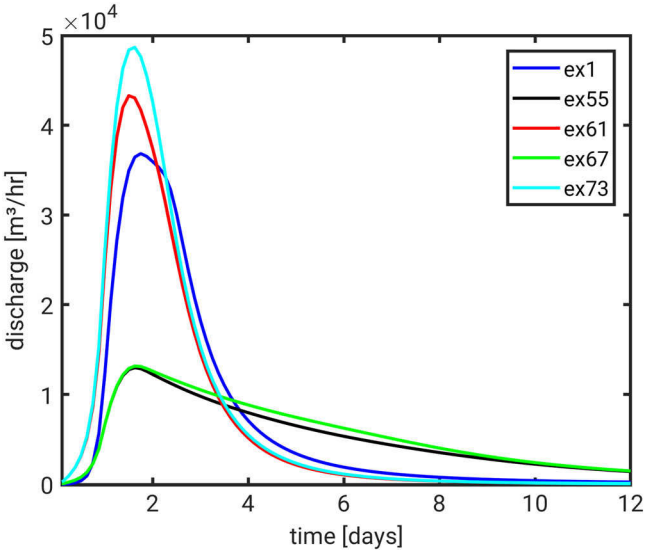

FIGURE 10 Hydrographs for the case with low rain rate (0.005 mm/hr) and WT = 0 m initial conditions for the 40 m case without scaling (ex1) and the 400 m cases without scaling (ex55), with Manning's scaling (ex61), with K_{sat} scaling (ex67) and both Manning's and K_{sat} scaling (ex73)

discharge is somewhat increased by reducing infiltration (NSC = −3.96). Scaling Manning's coefficient, however, largely increases the discharge peak and speeds up recession increases peak discharge above the 40 m simulation (NSC = 0.93). Scaling hydraulic conductivity as well further amplifies the discharge peak and total discharge increases (NSC = 0.90). For the 200 m resolution (Figure 11), scaling the Manning's coefficient alone yields results even closer to the 40 m resolution simulation (NSC > 0.98). For the high rain rate simulations (Figure 12), also the 400 m resolution with Manning's scaling leads to very good results (NSC > 0.99), whereas scaling only hydraulic conductivity barely has any impact (NSC = −0.77). For a low initial water table and low rain rate, scaling hydraulic conductivity becomes more important; without its scaling (whereas scaling Manning's) total discharge is significantly reduced at 400 m resolution and reduces the NSC from 0.90 to 0.87 (Figure 13).

5.2 | Semi-idealized Neckar test case

The results of the semi-idealized experiment with a single half-day precipitation event when scaling the Manning's coefficient alone

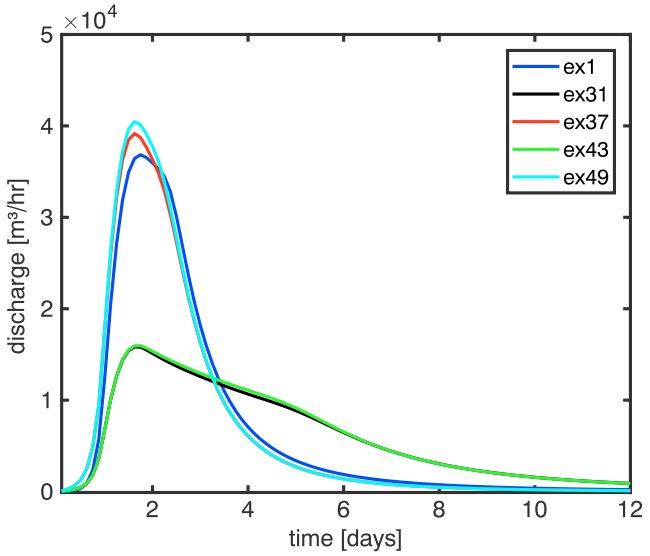

FIGURE 11 Hydrographs for the case with low rain rate (0.005 mm/hr) and WT = 0 m initial conditions for the 40 m case without scaling (ex1) and the 200 m cases without scaling (ex31), with Manning's scaling (ex37), with K_{sat} scaling (ex43) and both Manning's and K_{sat} scaling (ex49)

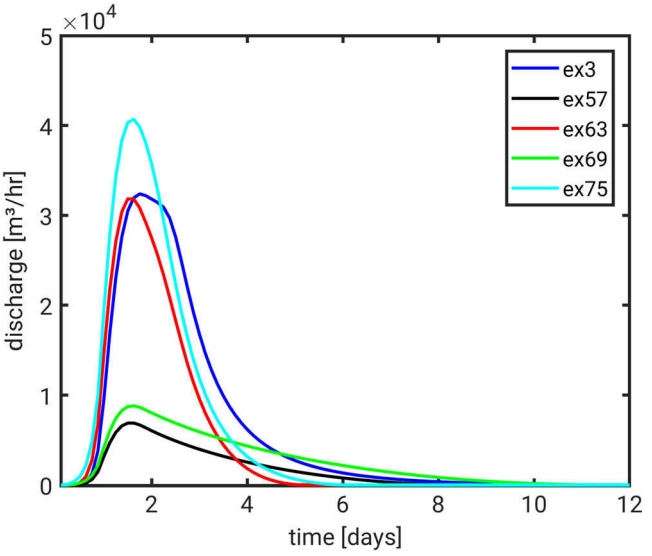

FIGURE 13 Hydrographs for the case with low rain rate (0.005 mm/hr) and WT = −5 m initial conditions for the 40 m case without scaling (ex3) and the 400 m cases without scaling (ex57), with Manning's scaling (ex 63), with K_{sat} scaling (ex69) and both Manning's and K_{sat} scaling (ex75)

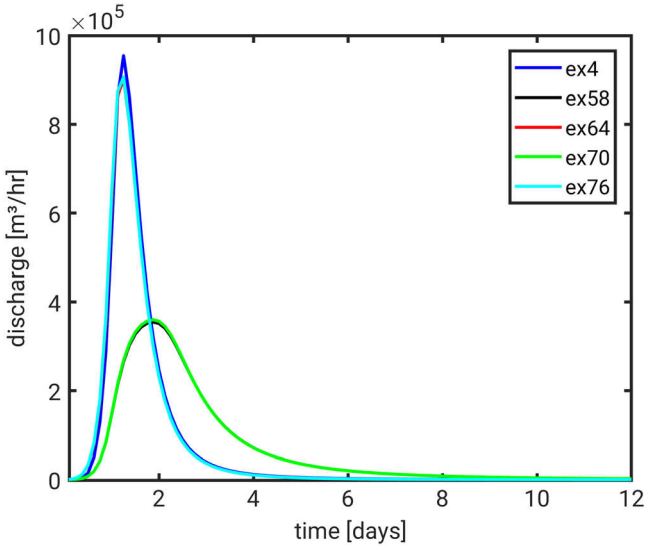

FIGURE 12 Hydrographs for the case with high rain rate (0.01 mm/hr) and WT = 0 m initial conditions for the 40 m case without scaling (ex4) and the 400 m cases without scaling (ex58), with Manning's scaling (ex64), with K_{sat} scaling (ex70) and both Manning's and K_{sat} scaling (ex76)

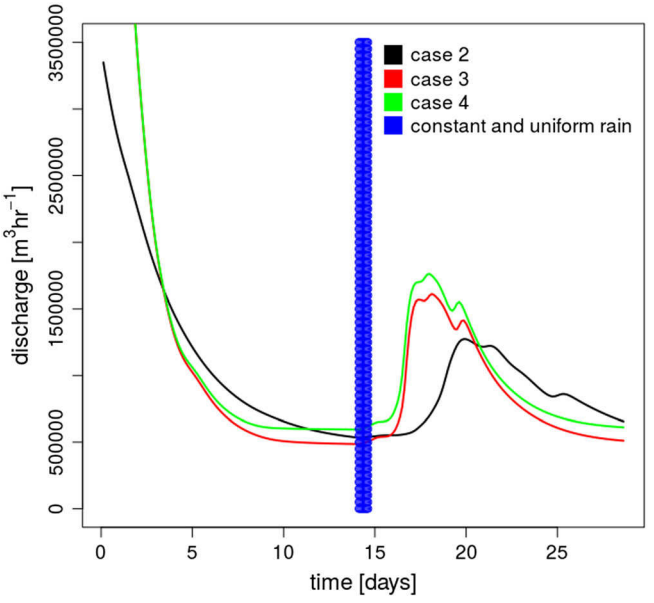

FIGURE 14 Hydrographs of the scaling experiments of the Nackar test case. Case2 = no scaling, case3 = Manning's scaling, case4 = Manning's and K_{sat} scaling

(case 3) and including the scaling of the saturated conductivity qualitatively (case 4) replicate the findings from the idealized catchment (Figure 14). The dry period in the beginning of the simulation removes potential footprints of past rain events. Scaling the Manning's coefficient enhances the discharge peak after the rain event (+25%) and shifts it earlier by 2 days. The additional scaling of the hydraulic conductivity further increases the discharge peak by 5% to 15%. Overall, these results compare well with those obtained for the ideal case for a high rain rate.

6 | DISCUSSION AND CONCLUSION

We suggest an improvement of river hydrographs simulated with the kinematic wave approach in distributed low hydrological models by

an objective scaling of the Manning's coefficient and saturated hydraulic conductivity. The ideal test case shows that scaling the Manning's coefficient positively impacts the simulated flood dynamics by bringing it in all cases closer to the expected discharge curve. For low rain rates and very low resolutions (about 10 times the grid spacing of the reference simulation), however, the peak discharge tends to be overestimated followed by a too fast recession. In almost all cases, it is advantageous to scale the Manning's coefficient with our approach.

Scaling the hydraulic conductivity does not exhibit such a clear benefit. The scaling reduces infiltration and thus leads to an overall higher discharge. This effect becomes very small at higher rain rates and/or for shallow initial water tables. For low rain rates and deep initial water tables, this scaling (when applied in addition to Manning's scaling) increases the discharge peak and might move the resulting discharge curve again further away from the reference. Thus, depending on the quantity of interest (e.g., the peak amplitude of a flood wave) it might be beneficial not to invoke the scaling of the hydraulic conductivity. The overall integrated discharge, however, is always improved by the scaling of the hydraulic conductivity.

The scaling study with the real world Neckar catchment should be interpreted with caution, because the size and slope of the real rivers can vary substantially from catchment to catchment. For this catchment scaling, the Manning's coefficient speeds up the response of the river to precipitation events and results in a faster recession during dry periods, as found for the ideal test cases. The implementation of the scaling approaches for real-world applications requires a more detailed sensitivity analysis of the effects of the estimated effective river widths, the chosen van Genuchten parameters, the scaling effects on the exchange between river and subsurface, and of the impact of the water table depth and the rain intensity and duration. Although we see an improvement in the response to the rain event, we have to acknowledge that the Neckar catchment is heavily managed, effects of which are not included in the simulations. Thus, we suggest to apply our approach in catchments with minimal human influence (see e.g., Caballero et al., 2007 or Pedinotti et al., 2012).

The choice of the threshold value for the computation of effective river widths W_1 in real catchments influences the number of river grid cells and the length of the river reaches in which scaling operations are performed. A higher threshold will reduce the scaled river cells and the length of the scaled river reaches, and vice versa. Thus, the choice of the threshold will also influence the propagation of the simulated flood waves. In ParFlow, smaller rivers may disappear completely during dry periods. Scaling of even these smaller rivers can lead to an improvement by keeping the river network as a whole; but the base flow of the larger rivers will only be marginally impacted. Although there is no objective lower limit, we recommend to refrain from river scaling, if either the river is not present over more than 50% of the simulated time in the unscaled experiment or if the river is that small that nonlinearities introduced by the riverbed morphology become important (width at and below 2 m). All this depends on the model resolution; as we could see in the idealized study, scaling becomes less successful for real channel width less than 1/10th of the grid resolution. Thus, the approach is likely not suitable for regions with pronounced seasonal variations in rainfall (monsoons or similar) which cause rivers to behave differently on longer timescales than typical floods in the mid-latitudes. Similarly, rivers that only appear due to heavy rain events cannot be scaled properly as there is not enough data to infer what the typical river width would be in that case.

Through the scaling of the saturated conductivity also soil moisture, base flow, and the infiltration/exfiltration between the river and the aquifer will be impacted. Following Darcy's equation (Equation (1b)), the vertical infiltration or exfiltration between river and aquifer depends on the hydraulic head gradient between the top soil layer of the river grid cell and the layer directly below. By scaling Manning's coefficient, the ponding depth is lower, which reduces the infiltration/exfiltration flux between river and aquifer and might even reverse its direction. These processes should be analysed in more detail for a real river network in search for an improved K_{sat} scaling, because our current approach neglects nonlinear interactions between river and subsurface. Our method might also lead to only little benefits, when the riverbed morphology—especially the width-discharge relation—largely differs from the empirical values we used, or when features like non-resolved waterfalls exist.

One last point of concern related to the way the rivers are simulated. Because of the low spatial resolution used in ParFlow, typical shapes of river valleys are not well represented, which affects also the stream-aquifer interaction since the model groundwater dynamics depends on the grid resolution (Refsgaard, 1997).

The developed methodology can be easily implemented in all models, which do not explicitly resolve the true river width for river routing when the width is known with reasonable accuracy. Practically only a preprocessing step is required, which does not increase computational demand during runtime. To our knowledge, no similar methods have been tried so far as most approaches rely on dedicated channel parameterizations that are much more complex to implement.

ACKNOWLEDGMENTS

The authors thank Fabian Gasper for his help to run ParFlow stand alone and fully coupled in TerrSysMP on the supercomputers of the Jülich Supercomputing Centre (2015). Special thanks go to Gabriele Baroni for additional support regarding overland flow in other models. Vincent Haefliger and Bernd Schalge were funded by the Deutsche Forschungsgemeinschaft (DFG) via the Research Unit FOR2131, sub-project C1. We also acknowledge support by the project Z4 of the DFG-funded Collaborative Research Center TR32 (Simmer et al., 2014) responsible for the development of TerrSysMP, by the Centre for High-Performance Scientific Computing in Terrestrial Systems of Geoverbund ABC/J The authors gratefully acknowledge the Gauss Centre for Supercomputing e.V. (www.gauss-centre.eu) for funding this project by providing computing time through the John von Neumann Institute for Computing (NIC) on the GCS supercomputers JUWELS and JUQUEEN at Jülich Supercomputing Centre (JSC, 2015).

ORCID

Bernd Schalge https://orcid.org/0000-0001-9757-8017
Vincent Haefliger https://orcid.org/0000-0001-7761-2900
Stefan Kollet https://orcid.org/0000-0003-0095-1554
Clemens Simmer https://orcid.org/0000-0003-3001-8642

REFERENCES

Baldauf, M., Seifert, A., Foerstner, J., Majewski, D., Raschendorfer, M., & Reinhardt, T. (2011). Operational convective-scale numerical weather prediction with the COSMO model: Description and sensitivities. *Monthly Weather Review*, *139*(12), 3887–3905. https://doi.org/10.1175/MWR-D-10-05013.1

Biancamaria, S., Andreadis, K. M., Durand, M., Clark, E. A., Rodríguez, E., Mognard, N. M., … Oudin, Y. (2010). Preliminary characterization of SWOT hydrology error budget and global capabilities. *IEEE Journal of Selected Topics in Applied Earth Observations and Remote Sensing*, *3*, 6–19. https://doi.org/10.1109/JSTARS.2009.2034614

Biancamaria, S., Lettenmaier, D. P., & Pavelsky, T. M. (2016). The SWOT mission and its capabilities for land hydrology. *Surveys in Geophysics*, *37*, 307–337. https://doi.org/10.1007/s10712-015-9346-y

Bürger, K., Dostal, P., Seidel, J., Imbery, F., Barriendos, M., Mayer, H., & Glaser, R. (2006). Hydrometeorological reconstruction of the 1824 flood event in the Neckar River basin (southwest Germany). *Hydrological Sciences Journal*, *51*(5), 864–877. https://doi.org/10.1623/hysj.51.5.864

Caballero, Y., Voirin-Morel, S., Habets, F., Noilhan, J., Le Moigne, P., Lehenaff, A., & Boone, A. (2007). Hydrological sensitivity of the Adour-Garonne river basin to climate change. *Water Resources Research*, *43*. https://doi.org/10.1029/2005WR004192

Clark, M. P., Bierkens, M. F. P., Samaniego, L., Woods, R. A., Uijlenhoet, R., Bennett, K. E., … Peters-Lidard, C. D. (2017). The evolution of process-based hydrologic models: Historical challenges and the collective quest for physical realism. *Hydrology and Earth System Sciences*, *21*, 3427–3440. https://doi.org/10.5194/hess-21-3427-2017

Clark, M. P., Fan, Y., Lawrence, D. M., Adam, J. C., Bolster, D., Gochis, D. J., … Zeng, X. (2015). Improving the representation of hydrologic processes in Earth system models. *Water Resources Research*, *51*, 5929–5956. https://doi.org/10.1002/2015WR017096

David, C. H., Habets, F., Maidment, D. R., & Yang, Z.-L. (2011). RAPID applied to the SIM France model. *Hydrological Processes*, *25*, 3412–3425. https://doi.org/10.1002/hyp.8070

David, C. H., Maidment, D. R., Niu, G.-Y., Yang, Z.-L., Habets, F., & Eijkhout, V. (2011). River network routing on the NHDPlus dataset. *Journal of Hydrometeorology*, *12*, 913–934. https://doi.org/10.1175/2011JHM1345.1

de Rooij, R. (2017). New insights into the differences between the dual node approach and the common node approach for coupling surface–subsurface flow. *Hydrology and Earth System Sciences*, *21*, 5709–5724. https://doi.org/10.5194/hess-21-5709-2017

Decharme, B., Alkama, R., Papa, F., Faroux, S., Douville, H., & Prigent, C. (2012). Global off-line evaluation of the ISBA–TRIP flood model. *Climate Dynamics*, *38*, 1389–1412. https://doi.org/10.1007/s00382-011-1054-9

Fang, Z., Bogena, H., Kollet, S., & Vereecken, H. (2016). Scale dependent parameterization of soil hydraulic conductivity in 3D simulation of hydrological processes in a forested headwater catchment. *Journal of Hydrology*, *536*, 365–375. https://doi.org/10.1016/j.jhydrol.2016.03.020

Foster, L. M., & Maxwell, R. M. (2019). Sensitivity analysis of hydraulic conductivity and Manning's n parameters lead to new method to scale effective hydraulic conductivity across model resolutions. *Hydrological Processes*, *33*, 332–349. https://doi.org/10.1002/hyp.13327

Gasper, F., Goergen, K., Shrestha, P., Sulis, M., Rihani, J., Geimer, M., & Kollet, S. (2014). Implementation and scaling of the fully coupled Terrestrial Systems Modeling Platform (TerrSysMP) in a massively parallel supercomputing environment-a case study on JUQUEEN (IBM Blue Gene/Q). *Geoscientific Model Development*, *7*, 2531–2543. https://doi.org/10.5194/gmd-7-2531-2014

Häfliger, V., Martin, E., Boone, A., Habets, F., David, C. H., Garambois, P.-A., … Biancamaria, S. (2015). Evaluation of regional-scale river depth simulations using various routing schemes within a hydrometeorological modeling framework for the preparation of the SWOT mission. *Journal of Hydrometeorology*, *16*, 1821–1842. https://doi.org/10.1175/JHM-D-14-0107.1

Jones, J. E., & Woodward, C. S. (2001). (2001): Newton-Krylov-multigrid solvers for large-scale, highly heterogeneous, variable saturated flow problems. *Advances in Water Resources*, *24*, 763–774. https://doi.org/10.1016/S0309-1708(00)00075-0

Jülich Supercomputing Centre (2015). JUQUEEN: IBM blue gene/Q supercomputer system at the Jülich supercomputing centre. *Journal of Large-Scale Research Facilities*, *1*(A1). https://doi.org/10.17815/jlsrf-1-18

Keune, J., Gasper, F., Goergen, K., Hense, A., Shrestha, P., Sulis, M., & Kollet, S. (2016). Studying the influence of groundwater representations on land surface-atmosphere feedbacks during the European heat wave in 2003. *Journal of Geophysical Research – Atmospheres*, *121*, 13, 301–13,325. https://doi.org/10.1002/2016JD025426

Kollet, S. J., & Maxwell, R. M. (2006). Integrated surface-groundwater flow modeling: A free-surface overland boundary condition in a parallel groundwater flow model. *Advances in Water Resources*, *29*, 945–958. https://doi.org/10.1016/j.advwatres.2005.08.006

Kurtz, W., He, G., Kollet, S., Maxwell, R., Vereecken, H., & Hendricks Franssen, H.-J. (2016). TerrSysMP-PDAF (version 1.0): A modular high-performance data assimilation framework for an integrated land surface–subsurface model. *Geoscientific Model Development*, *9*(4), 1341–1360. https://doi.org/10.5194/gmd-9-1341-2016

Ledoux, E., Girard, G., Marsily, G. D., & Deschenes, J. (1989). Spatially distributed modelling: Conceptual approach, coupling surface water and ground-water. In H. J. Morel-Seytoux (Ed.), *Unsaturated flow in hydrologic modelling: Theory and practice, NATO ASI Ser. C* (pp. 435–454). Mass: Kluwer Acad., Norwell. https://doi.org/10.1007/978-94-009-2352-2_16

Leopold, L. B., & Maddock, T. Jr. (1953). The hydraulic geometry of stream channels and some physiographic implications. *USGS Professional Paper*, *252*, 57.

Masson, V., Le Moigne, P., Martin, E., Faroux, S., Alias, A., Alkama, R., … Voldoire, A. (2013). The SURFEX v7.2 land and ocean surface platform for coupled or offline simulation of earth surface variables and fluxes. *Geoscientific Model Development*, *6*, 929–960. https://doi.org/10.5194/gmd-6-929-2013

Nash, J. E., & Sutcliffe, J. V. (1970). River flow forecasting through conceptual models part I—A discussion of principles. *Journal of Hydrology*, *10*, 282–290. https://doi.org/10.1016/0022-1694(70)90255-6

Neal, J., Schumann, G., & Bates, P. (2012). A subgrid channel model for simulating river hydraulics and floodplain inundation over large and data sparse areas. *Water Resources Research*, *18*(1–16), 2012. https://doi.org/10.1029/2012WR012514

Niedda, M. (2004). Upscaling hydraulic conductivity by means of entropy of terrain curvature representation. *Water Resources Research*, *40*, n/a–n/a. https://doi.org/10.1029/2003WR002721

Oleson, K. W., Niu, G. Y., Yang, Z. L., Lawrence, D. M., Thornton, P. E., Lawrence, P. J., & Qian, T. (2008). Improvements to the community land

model and their impact on the hydrological cycle. *Journal of Geophysical Research: Biogeosciences* (2005–2012), *113*(G1). https://doi.org/10.1029/2007JG000563

Pedinotti, V., Boone, A., Decharme, B., Crétaux, J. F., Mognard, N., Panthou, G., … Tanimou, B. A. (2012). Evaluation of the ISBA-TRIP continental hydrological system over the Niger basin using in situ and satellite derived datastes. *Hydrology and Earth System Sciences*, *16*, 1745–1773. https://doi.org/10.5194/hess-16-1745-2012

Piccolroaz, S., Di Lazzaro, M., Zarlenga, A., Majone, B., Bellin, A., & Fiori, A. (2016). HYPERstream: A multi-scale framework for streamflow routing in large-scale hydrological model. *Hydrology and Earth System Sciences*, *20*, 2047–2061. https://doi.org/10.5194/hess-20-2047-2016

Refsgaard, J. C. (1997). Parameterisation, calibration and validation of distributed hydrological models. *Journal of Hydrology*, *198*(1–4), 69–97. ISSN 0022-1694, https://doi.org/10.1016/S0022-1694(96)03329-X

Richards, L. A. (1931). Capillary conduction of liquids through porous media. *Physics*, *1*, 318–333. https://doi.org/10.1063/1.1745010

Schalge, B., Rihani, J., Baroni, G., Erdal, D., Neuweiler, I., Hendricks-Franssen, H., … Simmer, C. (2017). High-resolution virtual catchment simulations using integrated modeling. *Hydrology and Earth System Sciences Discussion*. https://doi.org/10.5194/hess-2016-557

Shrestha, P., Sulis, M., Masbou, M., & Simmer, C. (2014). A scale-consistent Terrestrial Systems Modeling Platform based on COSMO, CLM, and ParFlow. *Monthly Weather Review*, *142*, 3466–3483. https://doi.org/10.1175/MWR-D-14-00029.1

Shrestha, P., Sulis, M., Simmer, C., & Kollet, S. (2015). Impacts of grid resolution on surface energy fluxes simulated with an integrated surface-groundwater flow model. *Hydrology and Earth System Sciences*, *19*, 4317–4326. https://doi.org/10.5194/hess-19-4317-2015

Simmer, C., Thiele-Eich, I., Masbou, M., Amelung, W., Crewell, S., Diekkrueger, B., … Waldhoff, G. (2014). Monitoring and modeling the terrestrial system from pores to catchments–The transregional collaborative research center on patterns in the soil-vegetation-atmosphere system. *Bulletin of the American Meteorological Society*, *96*, 1765–1787. https://doi.org/10.1175/BAMS-D-13-00134.1

Sulis, M., Keune, J., Shrestha, P., Simmer, C., & Kollet, S. J. (2018). Quantifying the impact of subsurface-land surface physical processes on the predictive skill of subseasonal mesoscale atmospheric simulations. *Journal for Geophysical Research - Atmospheres*, *123*(17), 9131–9151. https://doi.org/10.1029/2017JD028187

Sulis, M., Williams, J. L., Shrestha, P., Diederich, M., Simmer, C., Kollet, S., & Maxwell, R. M. (2017). Coupling groundwater, vegetation, and atmospheric processes: A comparison of two integrated models. *Journal of Hydrometeorology*, *18*, 1489–1511. https://doi.org/10.1175/JHM-D-16-0159.1

Valcke, S. (2006): OASIS3 PRISM Model Interface Library: OASIS3 User Guide. PRIMS Support Initiative, Report No. 3.

Van Genuchten, M. T. (1980). A closed-form equation for predicting the hydraulic conductivity of unsaturated soils. *Soil Science Society of America Journal*, *44*, 892–898. https://doi.org/10.2136/sssaj1980.03615995004400050002x

Wood, E. F., Roundy, J. K., Troy, T. J., van Beek, L. P. H., Bierkens, M. F. P., Blyth, E., … Whitehead, P. (2011). Hyperresolution global land surface modeling: Meeting a grand challenge for monitoring Earth's terrestrial water. *Water Resources Research*, *47*. https://doi.org/10.1029/2010WR010090

Yamazaki, D., de Almeida, G. A. M., & Bates, P. D. (2013). Improving computational efficiency in global river models by implementing the local inertial flow equation and a vector-based river network map. *Water Resources Research*, *49*, 7221–7235. https://doi.org/10.1002/wrcr.20552

How to cite this article: Schalge B, Haefliger V, Kollet S, Simmer C. Improvement of surface run-off in the hydrological model ParFlow by a scale-consistent river parameterization. *Hydrological Processes*. 2019;33:2006–2019. https://doi.org/10.1002/hyp.13448